Appl. Phys. B 92, 459–465 (2008)
DOI: 10.1007/s00340-008-3086-3

Applied Physics B
Lasers and Optics

R. WEHR[1,✉]
S. KASSI[2]
D. ROMANINI[2]
L. GIANFRANI[1]

Optical feedback cavity-enhanced absorption spectroscopy for in situ measurements of the ratio $^{13}C : {}^{12}C$ in CO_2

[1] Dipartimento di Scienze Ambientali, Seconda Università di Napoli, Via Vivaldi 43, Caserta 81100, Italy
[2] Laboratoire de Spectrométrie Physique – CNRS UMR5588, Université J. Fourier de Grenoble, 140 Rue de la Physique, Batiment E45, 38402 St. Martin d'Hères, France

Received: 15 January 2008 / Revised version: 7 April 2008
Published online: 27 June 2008 •

ABSTRACT We report on the design and laboratory performance of a portable infrared absorption spectrometer for the measurement of the isotopic ratio $^{13}C : {}^{12}C$ in CO_2. The design relies on optical feedback cavity-enhanced absorption spectroscopy in the 2 μm spectral region to achieve optimal performance at ambient CO_2 concentrations. The prototype instrument measures $\delta^{13}C$, relative to a standard calibration bottle, with a precision of ±0.7‰ for a 20-s integration time and with an automatic recalibration every 6 min. The absolute accuracy obtained is 0.9‰. The principal performance limitations are discussed along with improvements currently being implemented for the second generation instrument.

PACS 42.62.Fi; 07.57.Ty; 33.20.Ea

1 Introduction

Respiratory and photosynthetic processes are known to discriminate to characteristic degrees between the stable carbon isotopologues of carbon dioxide – namely $^{12}CO_2$ and $^{13}CO_2$. For this reason, measurements of the isotopic composition of CO_2 gas can provide otherwise obscure information on carbon cycling and biological activity in ecosystems (see, for example, [1–4]). The standard method for such measurements has long been isotope ratio mass spectrometry (IRMS), which is generally sufficiently accurate and reliable for ecological research, determining $\delta^{13}C$ in CO_2 with uncertainties of less than 0.1‰.[1] The primary drawback of IRMS is that the analysis must be performed in the laboratory, and so samples must be collected in flasks and transported, which strongly limits both the temporal resolution and the overall number of samples for a field campaign. The secondary drawback of IRMS is that the analysis of each sample must be preceded by time-consuming sample preparation.

These drawbacks have spurred a suite of research into infrared spectroscopic methods for measuring $\delta^{13}C$ in CO_2 [5–16], as well as for measuring oxygen isotope ratios in CO_2 (e.g., [17, 18]) and various isotope ratios in other molecules (e.g., [19–24]). Since $^{12}CO_2$ and $^{13}CO_2$ each produces a distinct and well known set of infrared absorption lines whose intensities depend on the individual isotopologue concentration, it is possible to determine the relative (or even absolute) abundances of $^{12}CO_2$ and $^{13}CO_2$ from a single high-resolution absorption spectrum. This can be done essentially in real-time, on site, and without sample preparation. In contrast to IRMS, however, isotope ratio infrared spectroscopy is relatively immature: development continues on a range of instrumental strategies in order to explore the advantages and limitations of each. The immediate goal for applied research is usually to approach the accuracy and reliability of IRMS but with a short measurement time (i.e., seconds or minutes). To date two field-deployable instruments [10, 12] have made that claim for $\delta^{13}C$ in ambient CO_2. For other applications, accuracies of even 1‰ suffice, and development is focused instead on features like sensitivity. In any case, the longer term goal is to create and test possibilities for future gains in accuracy, sensitivity, time resolution, portability, robustness, ease of use, and so on. From the point of view of fundamental science, a no less important goal is the development of the experimental methodologies for their own sake.

The instruments described in [10, 12] both take advantage of the strong CO_2 absorption lines found in the mid-infrared region. Other CO_2 instruments have operated instead in the near infrared,[2] where the spectral lines tend to be orders of magnitude weaker, but where detectors and continuous-wave lasers are available at much lower cost, and without any need for cryogenic coolant for the laser or detector. The job of making up for the lost sensitivity in these instruments typically falls to some optical scheme for folding a long absorption path length into a compact instrument. One method is to use a Herriott-type multipass cell, as in [13, 15]. In this way, a half-meter cell can contain an optical path length of 20 or 30 m. Much more dramatic increases in the optical path length have been obtained by placing the gas inside a high-finesse optical cavity, where the average photon makes thousands of passes through the gas before "leaking" through the output mirror and reaching the detector. The fundamental difficulty

✉ Fax: +39-0823-274605, E-mail: rick.wehr@unina2.it

[1] The notation $\delta^n M$ refers to the ratio of the mass-n isotope of atom M to the most abundant isotope of atom M, expressed as a relative difference from an arbitrary standard.

[2] To our knowledge, only one such instrument [14] has been deployed in the field, for measurements of volcanic CO_2 at elevated concentrations.

with high-finesse cavities is that their transmission modes are generally much narrower than the laser linewidth, so that most of the laser power is filtered by the cavity and lost. Techniques that have been used to overcome this difficulty (not necessarily in CO_2) include off-axis integrated cavity output spectroscopy (OA-ICOS) [17, 20, 21] and optical feedback cavity-enhanced absorption spectroscopy (OF-CEAS) [22, 25, 26]. When applied to measurements of $\delta^{13}C$, these approaches have not yet achieved the accuracy of IRMS (at least not at the desired temporal resolution), but they hold great potential both for (1) practical improvements in the near future and (2) export to other molecules and other spectral regions, allowing for isotopic measurements at ultra-low concentrations or in particularly rare gases. Export to the mid-infrared in particular is becoming increasingly feasible as components in that region become more readily available. In fact the OA-ICOS technique has recently been implemented in the mid-infrared for isotopic measurements in stratospheric water vapor [20, 21].

Here we report on the first use of the OF-CEAS method for measuring $\delta^{13}C$ in CO_2 at ambient concentrations. The spectrometer features a high sensitivity for the near-infrared region, a relatively compact (portable) design and low cost, cryogen-free operation, and the possibility of absolute concentration measurements. It is our hope that the results presented might inform the development of other isotope ratio spectrometers, whether they be using OF-CEAS or another cavity-enhanced approach.

We begin in the next section by describing the instrument design. We then outline the data analysis procedure in Sect. 3, and report on the instrument's performance in laboratory trials in Sect. 4. Section 5 contains our discussion of the results, while planned improvements to the apparatus are described in Sect. 6.

2 Instrument design

The OF-CEAS technique has been well described by Morville et al. [25] and additional details on the analysis of OF-CEAS data for isotopic measurements have been given by Kerstel et al. [22]. We provide in this section a description of the particulars of our instrument along with some important points from [22, 25], for the reader's convenience.

The spectrometer's optical setup is mounted on a $50 \times 120\,cm^2$ breadboard and depicted in Fig. 1. The instrument operates by measuring the transmission of a Nanoplus DFB diode laser beam at 2.007 μm through a V-shaped[3] optical cavity with two 50 cm arms set at a 2° angle, while the laser frequency is ramped quasi-linearly at a repetition rate of 10 Hz over a spectral range of about 7 GHz. This range is just large enough to include the $R(17)e$, $21112 \leftarrow 01101$ line of $^{12}CO_2$ at $4978.2047\,cm^{-1}$ and the $P(16)e$, $20011 \leftarrow 00001$ line of $^{13}CO_2$ at $4978.0226\,cm^{-1}$. This line pair has two favorable features for isotope ratio determinations. First, the lines are closely spaced, allowing both to be measured in a single narrow laser scan, effectively simultaneously, and yet they are not so closely spaced as to overlap significantly. A narrow scan is desirable in order to enhance laser stability, increase the spectral sampling density, limit the burden placed on the piezoelectric phase control loop (see below), and reduce the change in laser output power that accompanies the frequency ramp (which is produced by a ramp in the laser driving current). The second favorable feature of this line pair is that the lines are of similar intensity after accounting for their natural abundances ($4.467 \times 10^{-23}\,cm^{-1}/(molecule\,cm^{-2})$ for the $^{12}CO_2$ line, and $7.074 \times 10^{-24}\,cm^{-1}/(molecule\,cm^{-2})$ for the other), enabling a good signal-to-noise ratio (SNR) to be obtained for both lines at the same gas pressure.

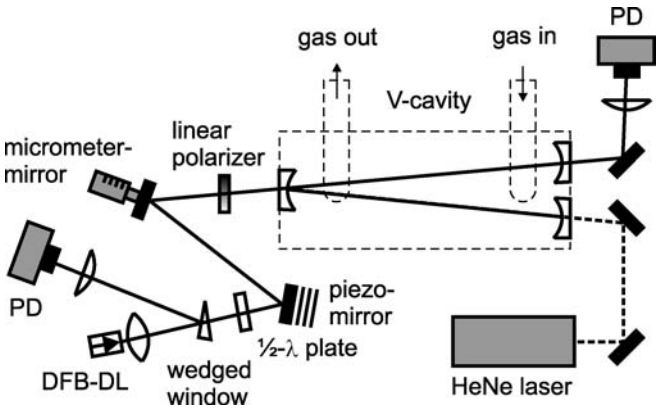

FIGURE 1 A diagram of the optical setup. The *solid black rectangles* indicate gold mirrors, and the *hollow planar-convex* or *biconvex shapes* represent the corresponding antireflection-coated lenses. PD stands for photodiode and DFB-DL for distributed-feedback diode laser

The optical cavity is created by three concave mirrors with radii of curvature of 1 m and an effective (weighted average) reflectivity of $R = 99.992\%$ at 2.007 μm, as determined from the empty cavity ringdown time, $20.5\,\mu s = -(l_1 + l_2)/(2c \ln R)$, where l_1 and l_2 are the lengths of the two cavity arms and c is the speed of light. For a V-shaped geometry, this reflectivity implies a cavity finesse $\mathcal{F} = \pi R/(1 - R^2) = 19\,500$, which corresponds to $12\,500\,(= 2\mathcal{F}/\pi)$ passes for the average photon and hence an effective optical path length of 12.5 km in the absence of absorption. The mirrors are mounted in stainless steel housings that fit (with vacuum-tight rubber o-rings) into the three tubular ends of a ∼ 1 l glass cell containing CO_2 gas diluted in air or nitrogen. The gas is injected into the cell through a pneumatic valve near the optical outputs, and exits through another such valve near the optical input (the folding mirror). In this way, the cell can be used in either a static or a flow configuration. For the purposes of these initial laboratory tests, the temperature was measured by a Pt100 precision platinum resistance thermometer mounted on the external surface of the glass cell, and the pressure was monitored (and maintained) by a pressure forward controller (PFC) immediately before the CO_2 input valve. The Pt100 was calibrated by the Italian National Institute of Metrological Research (INRiM) to within 10 mK. The pressure gauge in the PFC is accurate to within 0.2 mbar, although exact knowledge of the pressure is not critical for our isotope ratio determinations.

The laser-cavity distance is an important parameter in OF-CEAS, and in our setup is equal to the length of one cavity arm (i.e., 50 cm), so that we observe both the even and odd mode families as described in [25]. Our spectral reso-

[3] The V geometry prevents retro-reflection from the input mirror from returning to the laser and causing uncontrolled optical feedback.

lution is thus equal to the free spectral range (FSR) of the total (i.e., 100 cm) cavity, which is about 150 MHz. (The frequency accuracy, on the other hand, is far superior, being roughly equal to the cavity mode width, about 10 kHz.) We are able to adjust the laser-cavity distance to within $\sim 10\,\mu$m of the correct value using one of two gold steering mirrors before the cavity, which is mounted on a micrometer-adjust translation stage. This precise adjustment is necessary in order to obtain (nearly) the same shape for all the cavity modes in our spectral scan. The second gold steering mirror is mounted on a piezoelectric membrane for adjusting the distance still more precisely: as in [25], the membrane is connected to an electronic feedback circuit that maintains the phase of the optical feedback at the optimal value for constructive interference, based on the symmetry of the individual cavity modes. This adjustment is made in real-time, with a bandwidth of a few tens of hertz and a range of motion of several micrometers.

Between the laser and the cavity, three additional optical components improve the performance of the system. First, an antireflection-(AR-)coated lens situated a few millimeters from the laser diode focuses its beam in the center of the cavity, by which we mean 75 cm from the laser, to enhance mode matching. Secondly, a wedged window splits off 10% of the beam and directs it through a focussing lens to the monitor detector: an extended-wavelength InGaAs photodiode with a bandwidth of about 100 kHz, used to correct for variations in the cavity input power. After that, the combination of a rotatable half-wave plate and a linear polarizer is used to set the optimal optical feedback rate by attenuating the return (and also the forward) beam.

After the cavity, a gold steering mirror sends the beam from one of the two cavity output mirrors through a focussing lens to the main detector: another extended-wavelength InGaAs photodiode but with a bandwidth of 1.5 MHz. The other cavity output mirror is reserved for use during initial setup and maintenance as an input for a helium neon laser alignment beam. The signals from both the main and monitor detectors are digitized by a National Instruments USB-6251 data acquisition (DAQ) board sampling each channel at 400 kHz. The DAQ board is also used to send, when desired, a TTL signal that activates a laser current bypass circuit, which shuts the laser off effectively instantaneously. This shutoff circuit is useful for measuring the detector zero level, and especially for performing occasional cavity ringdown measurements, which are used to calibrate the OF-CEAS spectra's absorption scale as described in Sect. 3.

The gas handling system begins with a pair of electric valves to switch automatically between sample and standard gas inlets. The chosen gas then flows through the PFC into the cell. A small low-vacuum pump after the outlet of the cell provides the suction that drives the flow.

3 Data analysis procedure

Although the procedure by which isotope ratios may be calculated from OF-CEAS spectra is described in detail in [22], we review the procedure here in order to highlight the elements that will be relevant to our discussion in Sect. 5. The raw spectrum obtained in OF-CEAS is a comb of cavity transmission peaks, each broadened by the frequency locking effect of the optical feedback to the point that the detector signal never or only briefly drops to zero in between them (see Fig. 2). This broadening of the cavity modes in time means that, at a sampling rate of 400 kHz and with roughly 50 modes in a 0.1 s scan, hundreds of sample points describe each mode, and 10 or 20 of those will fall close enough to the flattened peak to contribute to a reliable calculation of its amplitude. (In contrast, without the frequency locking effect, the temporal full-width at half maximum amplitude of a cavity mode for the above scan parameters would be about 25 times shorter than the sampling interval.) In our case, the root-mean-squared noise in the raw detector signal is 1 mV while the mode peak amplitudes are around 1.5 V. The signal-to-detector-noise ratio in our calculated cavity mode peak amplitudes is therefore around 5000 : 1, although the overall absorption space SNR is limited at about 1500 : 1 relative to the peak amplitude of the $^{12}CO_2$ line (or 300 : 1 relative to the $^{13}CO_2$ line) by mechanical and acoustic vibrations. Once the peak amplitudes are calculated, they are divided by the corresponding signals from the monitor detector to normalize by the cavity input and thus obtain the peak fractional cavity transmission $H_{\max}(m)$ for each mode m.

The interpretation of these normalized transmission peaks is substantially more complicated in the case of OF-CEAS than it would be for simple linear absorption, where the Lambert–Beer law would suffice. Instead, it can be shown that absorption by an intracavity gas with absorption coefficient α_m at the peak of cavity mode m leads to fractional transmission maxima given by [25]:

$$H_{\max}(m) = \left[\frac{T\exp(-\alpha_m l_1/2)}{1 - R^2\exp(-\alpha_m(l_1+l_2))}\right]^2, \tag{1}$$

where $T = (T_v T_1)^{1/2}$ is the effective mirror transmission coefficient and $R = (R_v)^{1/2}(R_1 R_2)^{1/4}$ is the effective mirror reflectivity coefficient mentioned earlier. The subscripts 1, 2,

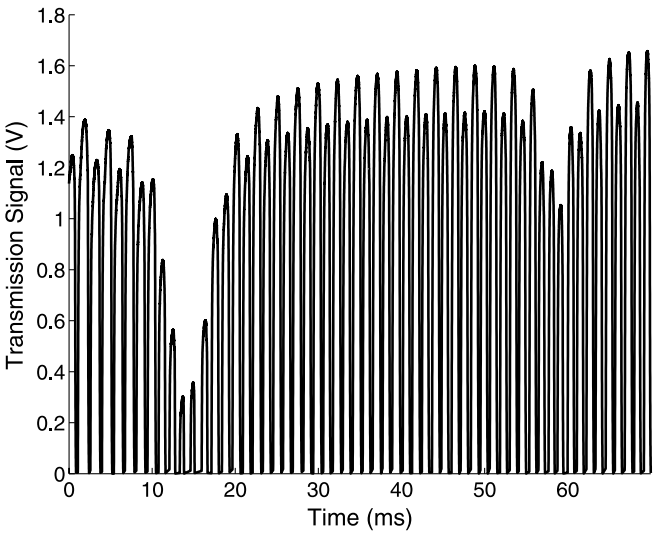

FIGURE 2 The raw transmission spectrum for a single laser scan, recorded with a digital sampling rate of 400 kHz and consisting of 58 cavity modes (29 "even" and 29 "odd") spaced at 150 MHz. The $^{12}CO_2$ (*left*) and $^{13}CO_2$ (*right*) absorption lines are clearly seen

and v refer to the mirrors at the ends of arms 1 and 2 and at the apex of the V, respectively.

Equation (1) can be inverted to yield, after some algebra and two good approximations [22]:

$$\alpha_m + \frac{\gamma_0}{c} = \frac{\gamma_m}{c} \approx \frac{T}{(l_1 + l_2)\sqrt{H_{\max}(m)}}\,, \tag{2}$$

where c is the speed of light, γ_0 is the loss coefficient for the empty cavity, and γ_m is the total loss coefficient at the peak of mode m. Equation (2) implies that it is possible to find α_m, apart from a constant offset γ_0/c, knowing only $H_{\max}(m)$ and the constant calibration factor $T/(l_1 + l_2)$. The latter can be determined if one knows both $H_{\max}(k)$ and γ_k for any single mode k, since it follows immediately from (2) that $T/(l_1 + l_2) = (\gamma_k/c)\sqrt{H_{\max}(k)}$. Fortunately, γ_k can be measured occasionally at one or even a number of modes by shutting off the laser at the cavity mode peak (using the current bypass circuit mentioned earlier) and fitting $\exp(-\gamma_k t)$ to the observed cavity ringdown.

The raw OF-CEAS spectrum is thus converted into a spectrum of α_m vs. m, to which one can fit a theoretical spectrum generated using a line shape function such as the Voigt. In our case, a Dicke-narrowed hard collision profile [27] yields a better fit to the data and so we use that. (The details of the line shape function are irrelevant for our purposes provided that it fits the measured line shapes within the noise.) A typical spectrum with fit residual is shown in Fig. 3. From each line shape fit, one can choose to retrieve either the absorption at the peak of the absorption profile, α_0, or the integrated area A underneath it, both of which are directly proportional to the number density of the corresponding isotopologue. In principle, the integrated area can be determined more robustly but requires a knowledge of the cavity FSR in order to convert the spectral abscissa correctly from mode number to frequency. Fortunately that is not a limitation in practice, because if one is interested only in isotope ratio measurements, and not in absolute concentrations, then any scaling error in the abscissa will cancel in the ratio and become irrelevant. (And for concentration measurements, the FSR could be calibrated relative to the absorption line separation, which is well known.) In any case, δ^{13}C is determined from either α_0 or A in exactly the same manner. This is generally done relative to a standard gas (i.e., one with a precisely known isotopic ratio) by periodically replacing the sample gas in the cell with the standard and calculating the super-ratio:

$$\delta^{13}\mathrm{C} = \frac{(A^{13}/A^{12})_{\mathrm{sam}}}{(A^{13}/A^{12})_{\mathrm{std}}} - 1\,, \tag{3}$$

where A^n is the integrated area (or, alternatively, the absorption at line peak) corresponding to the mass-n isotope of carbon, and where the subscripts "sam" and "std" refer to the sample and standard gases, respectively.

Because the ratio A^{13}/A^{12} (or $\alpha_0^{13}/\alpha_0^{12}$) depends on the gas temperature via the line strengths, any difference in the temperatures of the sample and standard gases will introduce an error into (3). The apparent variation $\Delta\delta$ in the isotope ratio caused by a temperature shift ΔT can be estimated to a good approximation by [24]:

$$\frac{\Delta\delta}{\Delta T} = \frac{\Delta E}{k_{\mathrm{B}} T^2}\,, \tag{4}$$

where k_{B} is the Boltzmann constant, T is the temperature, and ΔE is the difference in the ground state energies of the transitions associated with the $^{12}CO_2$ and $^{13}CO_2$ absorption lines. The one unfavorable property of our selected line pair is that ΔE is large, so that the ratio of the line intensities, and hence the retrieved isotopologue ratio, depends strongly on the temperature difference between the standard and sample gases. In fact, in our case, $\Delta E = 681\ \mathrm{cm}^{-1}$ and so (4) yields $\Delta\delta = 11.2‰/\mathrm{K}$. It is therefore necessary to measure temperature variations to within 10 mK if accuracies of 0.1‰ in δ^{13}C are to be achieved. In the present laboratory tests, temperature errors were not a problem, as the cell temperature was found to vary by less than 30 mK over 1 h. However, for field measurements, the Pt100 thermistor will be suspended inside the gas cell. Other intended improvements to the cell are discussed in Sect. 6.

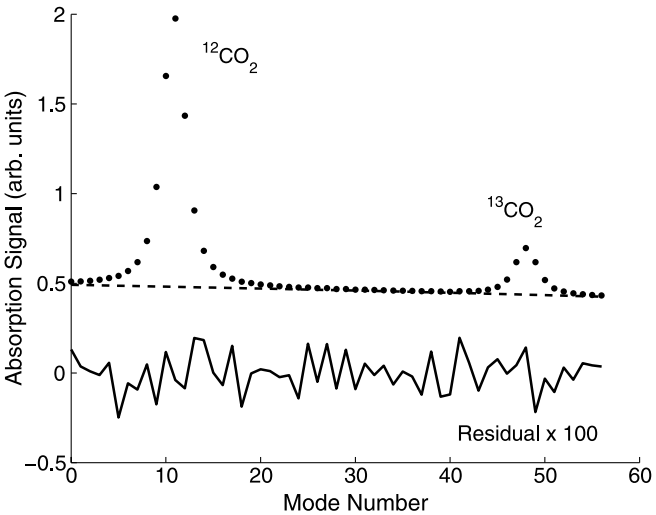

FIGURE 3 *Upper plot* shows a typical measured absorption spectrum (*dots*) and its fitted fourth order baseline (*dashed line*), whose curvature cannot be seen on this scale. *Lower plot* shows 100 times the corresponding fit residual, i.e., data minus fit, obtained from a hard collision profile

4 Testing and performance

The instrument was tested using bottled CO_2 at near-ambient concentrations. The total gas pressure was reduced to 80 mbar before entering the cell by the PFC. This low pressure reduces collisional broadening of the spectral lines to the point where they do not significantly overlap: the half-width at half maximum intensity of each line is about $0.01\ \mathrm{cm}^{-1}$ while their peak separation is $0.18\ \mathrm{cm}^{-1}$.

The first type of test was a static fill (i.e., no flow) trial designed to quantify the short- and long-term measurement precision. The cell was filled once with 500 ppm CO_2 in air and then sealed. This same gas fill was used as both the sample and the standard, so that the retrieved δ^{13}C ought to be zero. We treated the first 100 s of data as the standard and proceeded to observe the behavior of the retrieved δ^{13}C relative to that "standard" over 1 or 2 h. This process was repeated dozens of times between attempts to optimize the alignment, but the

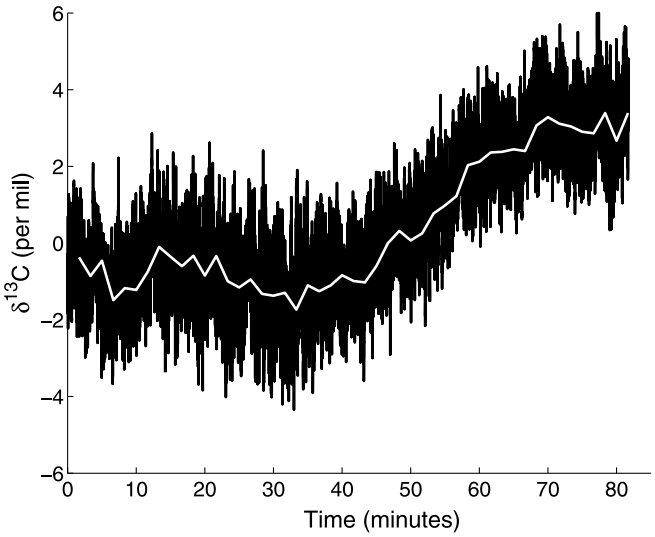

FIGURE 4 Variation in $\delta^{13}C$ retrieved from a single static gas fill over 80 min for a 1 s integration time (*black line*) and a 100 s integration time (*white line*). Values are relative to the isotopic ratio retrieved from the first 100 s of data

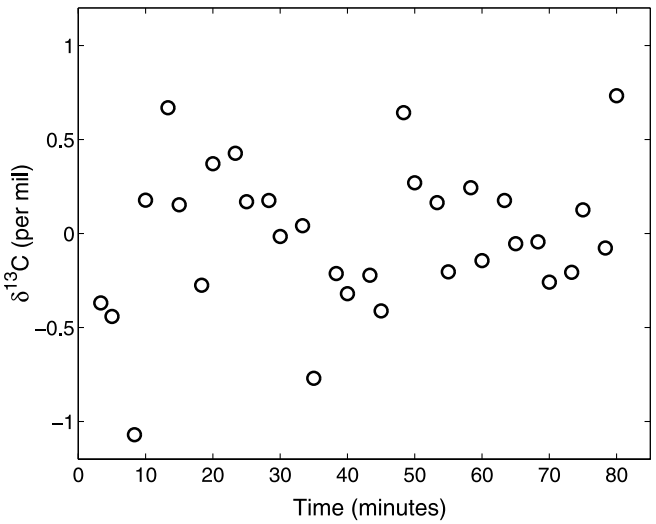

FIGURE 5 Retrieved $\delta^{13}C$ for a 100 s integration time with recalibrations every 5 min, using the same data as in Fig. 4

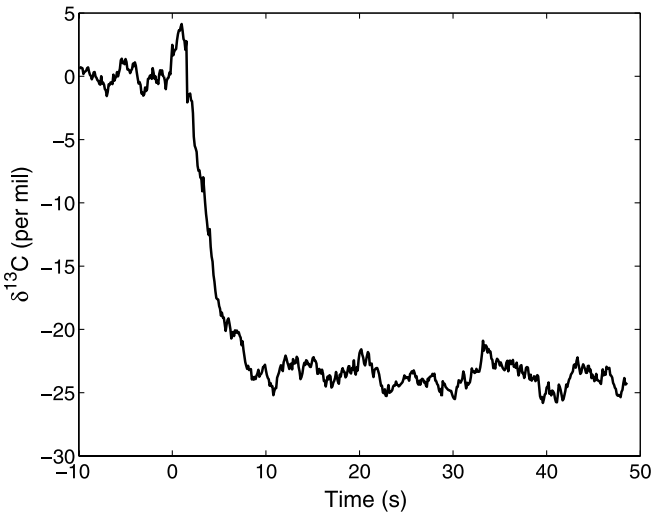

FIGURE 6 Transition (beginning at 0 s) of the retrieved $\delta^{13}C$ at the switching of the source gas from standard to sample. Values are relative to a preceding standard gas calibration. The integration time is 1 s

best results obtainable were always as follows. The short-term noise for a 1-s integration time was found to be $\pm 0.7‰\,(1\sigma)$, centered on zero. If this were the only noise present, it could be averaged out to $\pm 0.1‰$ over 1 min, which is a very fast temporal resolution for all but eddy covariance studies, and which is equal to the intended temporal resolution of the instrument. However, slower drifts were observed over several minutes. These drifts varied in magnitude, being sometimes absent and sometimes present at magnitudes as large as 1‰ per minute. A typical trial result is shown in Fig. 4. We return to the possible causes of the $\delta^{13}C$ drifts below.

To determine the efficacy of periodic calibrations in correcting for the long-term drifts, the same data acquired in the trials just described were analyzed differently. Each data set was divided into alternating "standard" and "sample" intervals, and each standard interval was used to calibrate the near halves of the sample intervals on either side (in this way, the longest time between a sample measurement and its calibration is only half the length of the sample measurement interval). A sample measurement was considered as the average of 1000 DAQ samples, or 100 s of data. Using a 5 min duty cycle consisting of a 100 s standard gas calibration and a 200 s sample gas interval (containing two 100 s measurements), the measurement precision was found to be $\pm 0.5‰\,(1\sigma)$ on average, although it varied from ± 0.3 to $\pm 0.7‰$ depending on the magnitude of the drifts in a given trial. An example of these results is shown in Fig. 5. Similar results are obtained when using a continuous flow in place of the single static fill.

The next type of test was a continuous flow trial designed to quantify the accuracy of the instrument. For this trial, the cell was left open and one of two bottled gas mixtures was flowed through it. One mixture was that used for the static fill precision test; its isotopic ratio had been measured at $-36.33 \pm 0.09‰$ (relative to the international PDB standard, $[^{13}C]/[^{12}C] = 1.12372 \times 10^{-2}$) using the IRMS at the Centre for Isotopic Research on Cultural and Environmental Heritage (CIRCE) in Caserta, Italy. The other mixture was of 400 ppm CO_2 in air, with an isotopic ratio certified at $-11.02 \pm 0.05‰$ by Australia's Commonwealth Scientific and Industrial Research Organisation (CSIRO). The flow was switched alternately from one bottle to the other using the electric valves described in Sect. 2, so that the CSIRO bottle could be considered the standard and the other the sample. For this test, the duty cycle was 120 s of standard followed by 240 s of sample. Note that this test further enabled us to quantify the gas exchange time for the cell: one can see in Fig. 6 that once the gas source is switched, the isotopic signature stabilizes at its new value after roughly 20 s (which becomes the practical limit on the spectrometer's temporal resolution). To avoid transitional effects, we therefore discarded the first 20 s of data in each sample or standard interval. The sample intervals were then further divided into a number of independent measurements dependent on the desired integration time. Figure 7 shows the delta values retrieved by this method over a period of 30 min, using integration times of 20 and 120 s. In both cases, we find a mean isotopic signature for the CIRCE bottle relative to

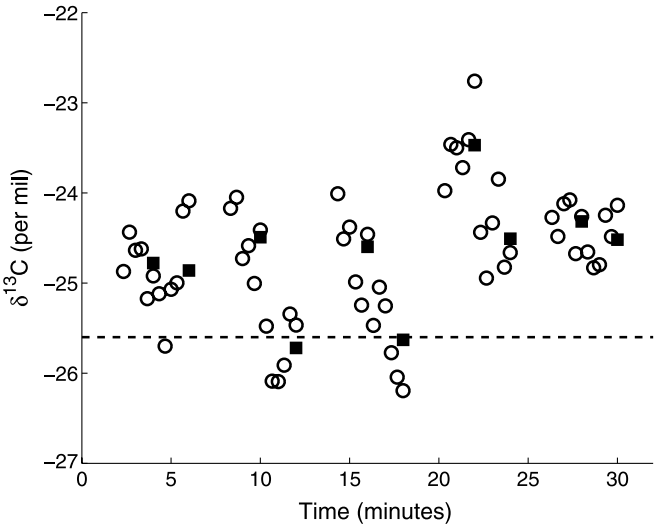

FIGURE 7 Retrieved δ^{13}C of the CIRCE sample gas relative to the CSIRO standard gas, for integration times of 20 s (*open circles*) and 120 s (*filled squares*), with 2-min long recalibrations every 6 min. The *dashed line* indicates the accepted IRMS value, $-25.6 \pm 0.1‰$

the CSIRO bottle of $\delta^{13}\mathrm{C} = -24.7‰$. The 1σ standard deviations (i.e., the statistical errors) in the individual isotope ratio determinations are ± 0.71 and $\pm 0.64‰$ for the 20 and 120 s integration times, respectively. Here the long-term drifting in δ^{13}C is clearly seen between calibrations, and is manifested in the fact that the precision does not improve substantially with the increased integration time. In fact, even with an integration time of only 2.5 s, the standard deviation is only $\pm 1.0‰$. These statistical errors are consistent with the error obtained in our static fill precision trials. Now, however, we also observe a systematic error of $+0.9‰$ in the average δ^{13}C when compared to the value calculated using the IRMS values for each bottle: $-25.6 \pm 0.1‰$ (note that this is not a simple difference between the PDB-referred values given above).

5 Discussion

The main limitation on the instrument performance is the drifting that occurs in the retrieved isotope ratio on a timescale of minutes; since that is the desired temporal resolution of the instrument, such drifts cannot be much reduced by averaging or by calibration. One potential cause of the drifts is the mechanical instability of the optical setup, particularly the cavity mirrors. However, we can find no correlation between drifts in the cavity length (observed as shifts in the cavity modes relative to the absorption lines) and the drifting of the retrieved δ^{13}C, making a strictly mechanical explanation for the drifts more difficult.

A second possible (and perhaps related) cause of the drifts arises from reflections from the back face of the cavity output mirror leading to the detector. The back faces of the cavity mirrors are neither wedged nor AR-coated, and we have found that the mirror substrate acts as an etalon, producing interference fringes with a wavenumber periodicity of just over $1\,\mathrm{cm}^{-1}$. Our usual $0.2\,\mathrm{cm}^{-1}$ scan is wide enough to see only a fraction of one of these fringes, which therefore appears as a curved baseline. We can account for the baseline with a fourth order polynomial during the line shape fitting, but the relatively large number of free fit parameters introduces the possibility of one parameter trading off with another nonphysically without significantly affecting the fit quality. Alternatively, small changes in the interference fringes (due to instabilities in the optical alignment) may be inducing variations in the retrieved line parameters. Indeed we have observed correlations between the high-order baseline parameters and the retrieved line absorptions. This is one potential explanation for the drifts that we observe in δ^{13}C.

Aside from problems in the line shape fitting algorithm, the interference fringes produced by the mirror substrates will introduce an error into the retrieved isotopic ratio because they induce a frequency-dependent loss in the cavity output signal that is (1) not seen by the monitor detector and (2) not reflected in the cavity ringdown time, which depends only on properties internal to the cavity. Thus our measured values of $H_{\max}(m)$ will be in error by a frequency-dependent factor, and the calibration factor $(\gamma_k/c)\sqrt{H_{\max}(k)}$ obtained from some particular mode k will no longer be valid for every mode m. The end result is that the mirror substrate fringes enter into the absorption spectrum as a frequency-dependent multiplicative scaling error. Unfortunately, the additive baseline included in the line shape fitting algorithm to account for the empty cavity loss term γ_0/c can never account for this error; it would be necessary to include simultaneously two kinds of baseline in the fitting: one additive and one multiplicative. But it is almost certain that some of the many baseline parameters involved in that case would be strongly correlated with the line absorptions, making reliable retrieval of α_0 or A impossible. The simpler solution to this problem would be to wedge and AR-coat the back faces of the cavity mirrors, an improvement currently being implemented for our next-generation instrument, as discussed below. Note that inasmuch as the mirror substrate fringe pattern is constant in time, it will contribute a systematic error to δ^{13}C (such as our $+0.9‰$ error), and inasmuch as the fringe pattern varies, it will enlarge the statistical uncertainty and/or the long-term drifts.

It is also possible that "short" fringes, with a scale approximately equal to our cavity mode spacing (or less), might be present in the spectra; such fringes would be very difficult to identify but could affect the retrieved line absorptions over time if the fringes drift relative to the absorption lines. Such fringes might be produced by spurious or diffuse reflection from one of the photodiodes or optics.

6 Future work

The principal improvement needed for the prototype instrument is the installation of cavity mirrors with wedged and AR-coated back faces. The use of such mirrors will eliminate the interference fringes produced in the mirror substrates, flattening the spectral baseline and therefore removing the most likely cause of systematic and statistical error. Another possible change to the apparatus would be the replacement of the glass cell with one of Zerodur® or stainless steel, to which the cavity mirrors would be permanently fixed for robustness during transport and for mechanical stability during operation. By drilling or milling the cell out of a Zerodur® or steel block, the cell volume can be reduced as

well, reducing the gas exchange time and hence improving the temporal resolution (a cell of this type is described in [22]). As has been mentioned, a Pt100 thermistor will be suspended inside the cell to allow for corrections to the retrieved isotopic ratios based on recorded differences between the standard and sample gas temperatures.

For the present tests at near-ambient CO_2 concentrations, there was no need to dilute the incoming gas; however, for ecological or medical studies involving respired CO_2, mixing ratios ranging from ambient up to about 0.01 would have to be adjusted to ambient levels for optimum operation. This dilution will be performed automatically by a split-path system before the cell, with one path containing a soda lime CO_2 filter, the other path being empty, and the proportion of the flow directed to each path adjusted in real-time by a pair of computer-controlled proportional valves.

7 Conclusion

We have presented a portable isotope ratio infrared spectrometer based on the OF-CEAS technique. In laboratory trials, the instrument measures $\delta^{13}C$ in CO_2 at ambient concentrations with a precision of $\pm 0.7‰$ and a systematic error of $+0.9‰$, given a temporal resolution of 20 s and a time between calibrations of 6 min. These figures are expected to be substantially improved by the installation of wedged cavity mirrors, as interference fringes in the cavity mirror substrates currently represent the most likely limit on instrument performance.

ACKNOWLEDGEMENTS We would like to thank the Marie Curie Transfer of Knowledge program for financial support of this research.

REFERENCES

1 J. Balesdent, A. Mariotti, B. Guillet, Soil Biol. Biochem. **19**, 25 (1987)
2 P. Ciais, P.P. Tans, M. Trolier, J.W.C. White, R.J. Francey, Science **269**, 1098 (1995)
3 L.B. Flanagan, J.R. Brooks, G.T. Varney, J.R. Ehleringer, Global Biogeochem. Cycl. **11**, 83 (1997)
4 D.R. Bowling, D.D. Baldocci, R.K. Monson, Global Biogeochem. Cycl. **13**, 903 (1999)
5 J.F. Becker, T.B. Sauke, M. Loewenstein, Appl. Opt. **32**, 1921 (1992)
6 D.E. Murnick, B.J. Peer, Science **263**, 945 (1994)
7 D.P. Cooper, R.U. Martinelli, C.B. Carlisle, H. Riris, D.B. Bour, R.J. Menna, Appl. Opt. **32**, 6727 (1993)
8 M. Erdélyi, D. Richter, F.K. Tittel, Appl. Phys. B **75**, 289 (2002)
9 E.R. Crosson, K.N. Ricci, B.A. Richman, F.C. Chilese, T.G. Owano, R.A. Provencal, M.W. Todd, J. Glasser, A.A. Kachanov, B.A. Paldus, T.G. Spence, R.N. Zare, Anal. Chem. **74**, 2003 (2002)
10 D.R. Bowling, S.D. Sargent, B.D. Tanner, J.R. Ehleringer, Agric. For. Meteorol. **118**, 1 (2003)
11 D. Weidmann, G. Wysocki, C. Oppenheimer, F.K. Tittel, Appl. Phys. B **80**, 255 (2005)
12 J.B. McManus, D.D. Nelson, J.H. Shorter, R. Jimenez, S. Herndon, S. Saleska, M. Zahniser, J. Mod. Opt. **52**, 2309 (2005)
13 G. Gagliardi, A. Castrillo, R.Q. Iannone, E.R.T. Kerstel, L. Gianfrani, Appl. Phys. B **77**, 119 (2003)
14 A. Castrillo, G. Casa, M. van Burgel, D. Tedesco, L. Gianfrani, Opt. Express **12**, 6515 (2004)
15 A. Castrillo, G. Casa, A. Palmieri, L. Gianfrani, Isotopes Environ. Health Stud. **42**, 47 (2006)
16 H. Wahl, B. Fidric, C.W. Rella, S. Koulikov, B. Kharlamov, S. Tan, A.A. Kachanov, B.A. Richman, E.R. Crosson, B.A. Paldus, S. Kalaskar, D.R. Bowling, Isotopes Environ. Health Stud. **42**, 21 (2006)
17 H.-J. Jost, A. Castrillo, H.W. Wilson, Isotopes Environ. Health Stud. **42**, 37 (2006)
18 A. Castrillo, G. Casa, L. Gianfrani, Opt. Lett. **32**, 3047 (2007)
19 C.R. Webster, A. Heymsfield, Science **302**, 1742 (2003)
20 E.J. Moyer, T.F. Hanisco, F.N. Keutsch, D.M. Sayres, N.T. Allen, J.M.S. Clair, E.M. Weinstock, J.R. Spackman, J.B. Smith, L. Pfister, T.P. Bui, J.G. Anderson, Ultra-sensitive isotope ratio measurements on atmospheric constituents. Presentation presented at International Conference on Field Laser Applications in Industry and Research (FLAIR) (2007)
21 E.J. Moyer, D.S. Sayres, T.F. Hanisco, J.M.S. Clair, F.N. Keutsch, N.T. Allen, G.S. Engel, J.H. Kroll, J. Paul, J.G. Anderson, submitted to this issue of Appl. Phys. B (2008)
22 E.R.T. Kerstel, R.Q. Iannone, M. Chenevier, S. Kassi, H.-J. Jost, D. Romanini, Appl. Phys. B **85**, 397 (2006)
23 D.W.T. Griffith, I. Jamie, M. Esler, S.R. Wilson, S.D. Parkes, C. Waring, G.W. Bryant, Isotopes Environ. Health Stud. **42**, 9 (2006)
24 P. Bergamaschi, M. Schupp, G.W. Harris, Appl. Opt. **33**, 7704 (1994)
25 J. Morville, S. Kassi, M. Chenevier, D. Romanini, Appl. Phys. B **80**, 1027 (2005)
26 S. Kassi, M. Chenevier, L. Gianfrani, A. Salhi, Y. Rouillard, A. Ouvrard, D. Romanini, Opt. Express **14**, 11 442 (2006)
27 P.L. Varghese, R.K. Hanson, Appl. Opt. **23**, 2376 (1984)